Electromagnetic Funnel: Reflectionless Transmission and Guiding of Waves through Subwavelength Apertures

Nasim Mohammadi Estakhri,[1,*] Nader Engheta,[1,†] and Raphael Kastner[1,2,‡]
[1]University of Pennsylvania, Philadelphia, Pennsylvania 19104, USA
[2]Tel Aviv University, Tel Aviv, 69978 Israel

(Received 31 May 2019; published 22 January 2020)

Confining and controlling electromagnetic energy typically involves a highly resonant phenomenon, especially when subwavelength confinement is desired. Here, we present a class of nonresonant, self-dual planar metastructures capable of protected energy transmission from one side to the other, through arbitrarily narrow apertures. It is shown that the transmission is in the form of matched propagating modes and is independent of the thickness and specific composition of the surface. We analytically prove that the self-dual condition is sufficient to guarantee 100% transmission that is robust to the presence of discontinuities along the propagation path. The results are confirmed numerically through study of various scenarios. The operation is broadband and subject only to the bandwidth of the constituent materials. The polarization of the internal field can also be independently controlled with respect to the incident one. Our structures are promising for applications in sensing, particle trapping, near-field imaging, and wide scan antenna arrays.

DOI: 10.1103/PhysRevLett.124.033901

It is well known that the interface between two structures with different compositions and constituent materials naturally entails a portion of incident electromagnetic (EM) energy to be reflected back toward the source. The reflection can, however, be reduced or fully eliminated through "matching" the interfaces, which is typically possible over a narrow frequency range [1,2]. In situations when engineering the transmission spectrum of a surface is sought for, the internal field distribution in the medium is not of particular importance. For instance, planar free-space filters (color filters, frequency selective surfaces, etc. [3–5]) may create complex and unpredictable near fields that strongly depend on their structural geometry and materials. On the other hand, the ability to control the field distribution across a surface while maintaining high throughput, also triggers several potential applications. As an example, creation of localized hot spots for EM energy in free space is quite challenging and very high numerical aperture lenses or complex structures are required to focus energy in nearly diffraction-limited spots [6–8]. However, it is known that a perforated metallic screen with subwavelength holes can be properly designed to be matched with free space and enable such localized enhanced field intensities on the surface, albeit for a narrow range of frequencies, promising for applications in opto-electronics and optical devices [9].

A relevant question that we address in this Letter is whether it is fundamentally possible to design planar slablike structures through which electromagnetic energy can be funneled along arbitrarily shaped, and particularly deeply subwavelength apertures and at the same time remain fully matched to free space. We do not impose any restrictions on the thickness of the slabs; i.e., we are considering configurations ranging from ultrathin plates with zero thickness to electromagnetically thick slabs. A related phenomenon that has been extensively studied in the past two decades is the case of extraordinary optical transmission (EOT) through subwavelength hole arrays. EOT introduced a new potential mechanism for concentrating EM energy at the subwavelength scale, as the light transmission through these hole arrays exceeds the Bethe limit [10], and even reaching 100% efficiency [11–15]. The high throughput apertures and the locally enhanced intensities prompted applications in chemical and bio sensors [16,17], photo emitters and detectors [18–20], enhanced Raman spectroscopy [21,22], lasers [23–25], photonic elements [9,26,27], nonlinear optical devices [28–30], and high resolution photolithography [31,32]. The physical mechanism behind the high level of transmission in EOT have been argued to be related to the existence of leaky surface modes (surface plasmons) coupling through evanescent waveguide modes present in the subwavelength holes [12,14,33]. The evanescent transmission through below cutoff holes, however, creates an exponential decay in the transmission amplitude as the thickness of such surfaces is increased [33]. In a quite different context, perfectly matched layers or absorbing layers have been studied for applications in numerical simulations and software packages to truncate the simulation domains. Rooted in their application, the core property of such artificially constructed materials is to remain matched to free space over a wide range of incident angles and

frequencies [34–36]. Matching is achieved through balancing electromagnetic properties of the material typically combined with a gradual increase in the loss coefficients. Checkerboard type configurations with electric-only and magnetic-only regions have also been studied in the past and reported in the literature as an approximation of such absorbing layers and Weston's [37] impedance matching condition [38–40].

Here, we propose a general class of planar configurations that are matched to free space under normally incident plane wave excitation; i.e., the reflection coefficient (backscattered power) is exactly zero. Matching across the interfaces as well as across all cross sections within the slabs is independent of the specifics of their patterning or their constituent materials, as long as they satisfy a certain duality condition discussed below. As shown in Fig. 1(a), we assume a two-dimensionally periodic planar arrangement of electrically polarizable (materials with $\varepsilon_r \neq 1$) and magnetically polarizable ($\mu_r \neq 1$) regions. Unit cells are in the cross sections (x-y plane) of the slabs, with

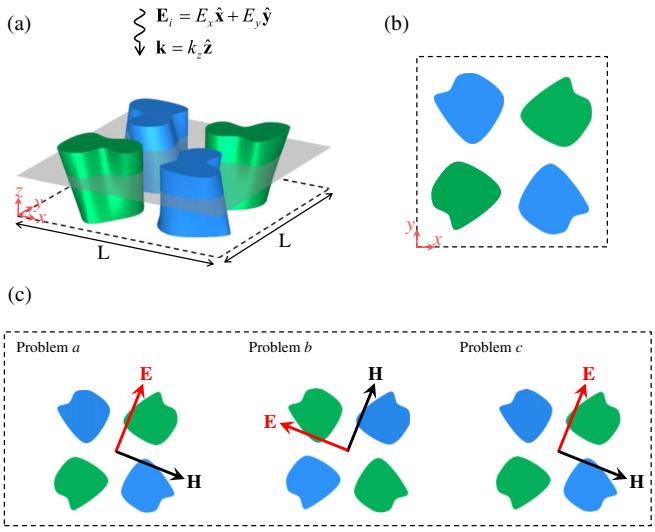

FIG. 1. Self-dual periodic slabs. (a) Conceptual representation of the unit cell of a self-dual slab, infinitely extended in the x and y directions with period L. Green and blue represent regions with electrically polarizable ($\varepsilon = \varepsilon_0\varepsilon_r$, $\mu = \mu_0$) and magnetically polarizable ($\varepsilon = \varepsilon_0$, $\mu = \mu_0\mu_r$) materials, assuming $\varepsilon_r = \mu_r$. Each unit cell is invariant under a 90° rotation around the z axis and swapping electric and magnetic materials. For simplicity, the case of only two materials in shown here. A horizontal z cross-section cut of the geometry along the gray surface is shown in panel (b). Cross section of the slab may arbitrarily vary between layers in terms of both shape and material properties, as long as the self-dual condition in Eq. (1) is satisfied (see examples in Ref. [41]). (c) Illustrations of three problems used in our proof: problem a, the original cross section; problem b, the dual of "problem a" constructed by changing the properties of constitutive materials and fields, according to duality theorem [42]; and problem c, 90° rotation of "problem b"(clockwise rotation is shown; the counterclockwise rotation follows similar formulation).

equal periods "L" in both directions and the origin of the local coordinates is placed at the center of this unit cell. The composition of the structure in the unit cell may also vary for different values of $z = z_0$; i.e., it does not require to be z invariant. We define such unit cell to be "self-dual" if the following condition is satisfied for the relative permeability and the relative permittivity at any $z = z_0$:

$$\varepsilon_r(x, y) = \mu_r(\pm y, x). \tag{1}$$

Inspecting Eq. (1), this condition defines a class of planar unit cells that remain *unchanged* if (i) the structure is rotated 90° around the z axis, and (ii) any electric material with relative permittivity ε_r is replaced by a magnetic material with relative permeability $\mu_r = \varepsilon_r$, and vice versa. The distributions of ε_r and μ_r are thus related through C_4 rotational symmetry. A simple case of such a cross section is shown in Fig. 1(b), in which only two different materials in each unit cell are considered (for more general examples see the Supplemental Material [41]). Here, we focus on *periodic* self-dual surfaces; however, the subsequent proof is general and valid for any *nonperiodic* (i.e., even single) self-dual scatterer as well. In such cases, the far-field scattering pattern of the self-dual element has a null in the backscattering direction.

We now prove the following statement: if we take a generic slab whose cross sections, including the interfaces, satisfy the self-duality condition in Eq. (1) it will produce zero backscattered field for arbitrarily polarized normally incident waves. Let us assume a normally incident plane wave—propagating in the negative z direction and with electric and magnetic field amplitudes defined as ($\mathbf{E}^{\text{inc}}$, $\mathbf{H}^{\text{inc}}$), in which each vector lies in the x-y plane. The backscattered far field (i.e., wave traveling along the $+z$ axis) is then a spherical wave with the amplitudes $e^{ikz}/kz(\mathbf{E}^{\text{back}}, \mathbf{H}^{\text{back}})$. Defining the 2×2 scattering matrices $\underset{=}{S}_{\mathbf{E}}$, $\underset{=}{S}_{\mathbf{H}}$ [43], the relation between the backscattered and incident wave amplitudes is

$$\mathbf{E}^{\text{back}} = \underset{=}{S}_{\mathbf{E}} \cdot \mathbf{E}^{\text{inc}}, \qquad \mathbf{H}^{\text{back}} = \underset{=}{S}_{\mathbf{H}} \cdot \mathbf{H}^{\text{inc}}. \tag{2}$$

It is straightforward to derive a general relation between $\underset{=}{S}_{\mathbf{E}}$ and $\underset{=}{S}_{\mathbf{H}}$ for an arbitrary scattering body [41]. For the self-dual structure, we evoke the duality theorem [42], followed by a 90° rotation operator [see Fig. 1(c)]. Assuming problems "a" and "b" corresponding to the original and dual cases, respectively,

$$\mathbf{H}_b^{\text{back}} = \frac{1}{\eta}\mathbf{E}_a^{\text{back}}, \qquad \mathbf{E}_b^{\text{back}} = -\eta\mathbf{H}_a^{\text{back}}. \tag{3}$$

By virtue of self-duality, the dual problem b is also obtained by a 90° rotation operator, i.e., problem c (e.g., for the incident field, with similar expressions for the reflected fields),

$$\mathbf{E}_c^{\text{inc}} = \pm\hat{\mathbf{z}} \times \mathbf{E}_b^{\text{inc}}, \qquad \mathbf{H}_c^{\text{inc}} = \pm\hat{\mathbf{z}} \times \mathbf{H}_b^{\text{inc}}, \tag{4}$$

in which the ± signs indicate 90° counterclockwise or clockwise rotation in the x-y plane, respectively. Self-duality ensures that problems "c" and "a"are identical [see Fig. 1(c)]. Combining Eqs. (1), (3), and (4) yields an additional relation between $\underline{\underline{S}}_{\mathbf{E}}$ and $\underline{\underline{S}}_{\mathbf{H}}$ [41], which cannot hold simultaneously with the previously derived condition, unless

$$\underline{\underline{S}}_{\mathbf{E}} = \underline{\underline{S}}_{\mathbf{H}} = \underline{\underline{0}}, \tag{5}$$

proving the above statement.

The results derived in Eq. (5) have an interesting implication for a periodic self-dual structure: the specular reflection coefficients (for both co- and cross polarizations) are exactly zero under normally incident plane wave illumination. In other words, independently of the geometrical details of the slab or the materials used in constructing the unit cell of the periodic structure, as long as the self-duality condition is satisfied, the surface remains matched to normally incident plane waves of arbitrary polarization. Indeed, values of permittivity or permeability may even change between different cross sections, yet the zero-reflection condition will always be satisfied. If the period of the cross section is smaller than a wavelength, i.e., only zeroth-order Floquet harmonics are present in the scattering response, it is implied that the entire incident energy must be transported through the slab. If higher order Floquet modes are present, Eq. (5) implies zero coupling into zeroth order reflection harmonics while some portion of power may couple to higher order reflection or transmission modes (see more discussion in Ref. [41]). Furthermore, the proof does not impose any restrictions on the local material properties, and they might be chosen as general as possible. For instance, permittivities and permeabilities might be both lossy (with the balanced conductivity in accordance with self-duality condition), implying absorption in the surface without reflection. With proper design, it is also expected that a self-dual arrangement be able to absorb the entire incident energy. From a physical point of view, the full cancellation of backscattering is enabled through destructive scattering from electric and magnetic elements. Exploiting two independent sets of elements (i.e., those supporting electrics current and those supporting magnetic ones) along with the structural symmetry allowed us to enforce zero backscattering. This approach is closely related to previous reports on controlling transmission and distribution, absorption, and confinement of electromagnetic waves using proper degrees of freedom in the system [44–47].

To further elucidate the implications of the above statements, we start by studying a generic slab with self-dual cross sections shown in Fig. 2(a). The unit cell is chosen to have a rather arbitrary profile, emphasizing the generality of the matching condition in Eq. (1). Each unit cell consists of eight cylinders with trapezoidal and circular cross

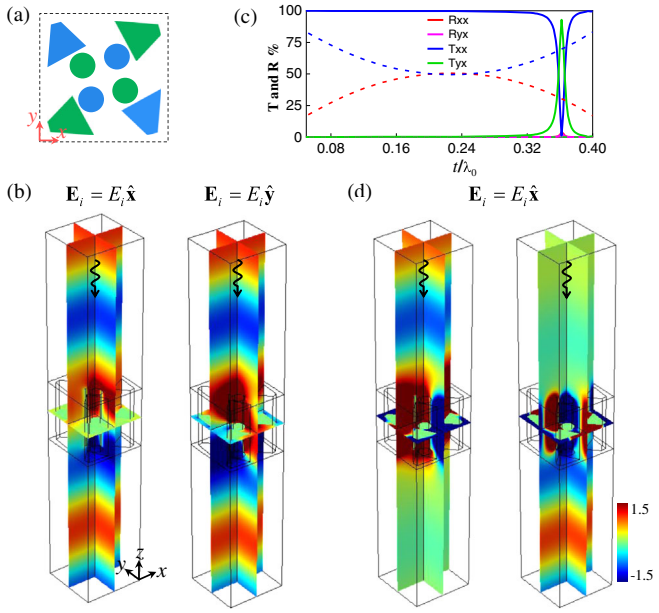

FIG. 2. Matching and polarization conversion in a generic self-dual periodic slab. (a) Unit cell of a generic self-dual slab with period of $L = 0.4\lambda_0$ in both the x and y directions. Green and blue represent regions with perfect electric conductor and perfect magnetic conductor boundaries, respectively. For simplicity, the slab is invariant along the z direction between the interfaces at $z_1 = -t/2$ and $z_2 = t/2$, where $t = 0.4\lambda_0$. More general cases including z-variant structures are studied in Ref. [41]. (b) Snapshot in time of the electric field distribution when the slab in panel (a) with $t = 0.4\lambda_0$ is illuminated with a plane wave propagating along the negative z direction. In each case, the component of the electric field parallel to the incident electric field is shown. Fields are normalized to the amplitude of the incident wave [color bar shown in panel (d)] and both cases are fully matched. (c) Reflected and transmitted powers from the slab shown in panel (a) (solid lines) vs its PEC counterpart, which is not self-dual (dashed lines) when illuminated with a $\hat{\mathbf{x}}$-polarized plane wave propagating along the negative z direction. (d) Snapshot in time of the x component (left) and y component (right) of the electric field, when the slab is illuminated with $\mathbf{E}_i = E_i\hat{\mathbf{x}}$ and $t = 0.362\lambda_0$. At this specific thickness, the transmitted wave experiences 90° polarization rotation, while matching is maintained.

sections, maintained between $z_1 = -t/2$ and $z_2 = t/2$. We consider an extreme case of self-duality condition; i.e., we assume the electric materials are perfect electric conductors (PEC) shown by green in Fig. 2(a), and the magnetic materials are perfect magnetic conductors (PMC), indicated by blue. The lattice period is fixed at $L = 0.4\lambda_0$ in both directions, thus ensuring only zeroth order Floquet harmonics to be excited in the far field. Full-wave numerical simulations [48] are used to calculate reflection and transmission coefficients for orthogonal linear polarizations of the incident wave when t is assumed to be $0.4\lambda_0$. As we expect, self-duality ensures full transmission in both cases [electric field distributions portrayed in Fig. 2(b)], in spite

of strong local field interactions of the incident wave and the electromagnetically thick slab. In this special case, since the scattering bodies are perfect conductors, the entire energy is flowing between the pillars and into the opposite interface of the slab. Counterpart examples of dielectric-based structures are discussed in detail in Ref. [41].

Interestingly, in spite of strong localized excitation of cross-coupled fields around the scatterers, the far-field interpolarization coupling is negligible, and the transmitted wave maintains the polarization of the incident wave, as shown in Fig. 2(b). While this may appear to be the consequence of the matching condition derived in Eq. (5), we note that the proof does not enforce conservation of polarization. Indeed, it should be possible, in principle, to couple the entire incident energy into the orthogonal transmitted polarization. To further investigate this possibility we change the thickness of the surface between $t = 0.02\lambda_0$ and $t = 0.4\lambda_0$, while looking at the percentage of the power coupled to co- and cross-polarized waves (T_{xx} and T_{yx} for illumination with $\hat{\mathbf{x}}$-polarized plane wave). Results are reported in Fig. 2(c).

First, we note that the total reflection is indeed zero, except for approximately 6% reflection around the resonance point at $t = 0.362\lambda_0$. This small reflection is attributed to numerical errors and mesh refinement at PEC/PMC corners [41]. At this resonant length, a complete polarization conversion is attained (i.e., $|T_{xx}| \to 0$ and $|T_{yx}| \to 1$), as shown in the field distributions of Fig. 2(d), yet matching is still preserved. The possibility of managing the outgoing polarization state without creating unwanted reflection can be of great interest for compact, tunable optical elements.

For comparison, we also looked at the nondual corresponding geometry where all the conductors are PEC. As expected, in the non-self-dual case the structure is not matched and a portion of the power is reflected back. This is shown with dashed lines in Fig. 2(c), highlighting the drastic difference between the response of self-dual and all PEC surfaces, although both consists of impenetrable perfect conductors of the same shapes and sizes. It is quite insightful to describe the observed zero backscattering phenomenon as an "impedance matching" condition, in accordance with scatterers that satisfy the generalized

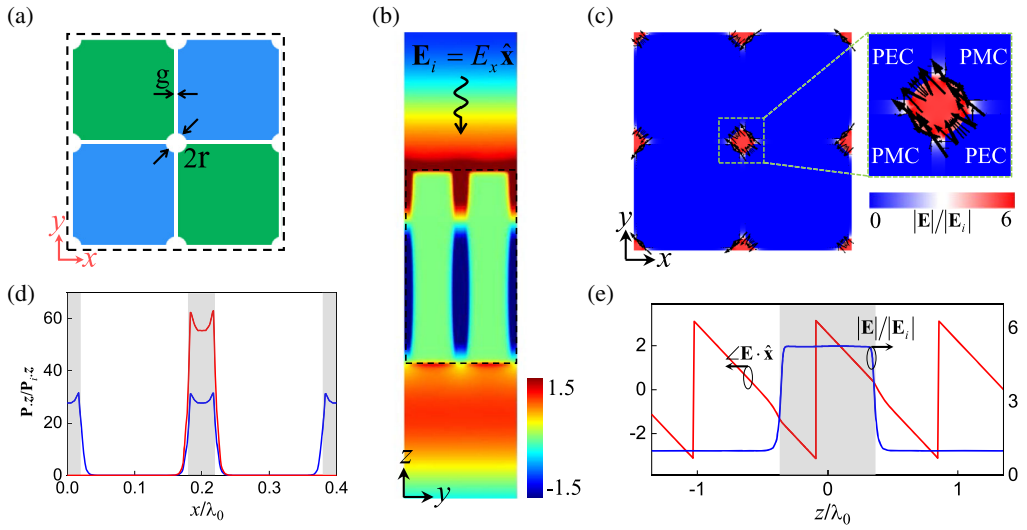

FIG. 3. Electromagnetic funnel: Reflectionless transmission of energy through deeply subwavelength apertures. (a) A horizontal cut of the unit cell of the self-dual periodic slab designed to transmit the EM energy through narrow air apertures (white). The period of the surface is $L = 0.4\lambda_0$ in both the x and y directions with $r = 0.02\lambda_0$, $g = 0.01\lambda_0$. Green and blue represent regions with PEC and PMC boundaries and the structure is invariant along the z direction between $z_1 = -t/2$ and $z_2 = t/2$, where $t = 0.7\lambda_0$. (b) Snapshot in time of the x component of the electric field distribution when the structure is illuminated with an $\hat{\mathbf{x}}$-polarized plane wave propagating along the negative z direction. Amplitude of the field is normalized to the incident wave. (c) Total field enhancement inside the narrow apertures. Polarization of the field in the center aperture is shown in the inset. Depending on the arrangement of PEC and PMC segments in the unit cell, each aperture supports a TEM-like mode with 45° tilted polarization. Because of illumination with an $\hat{\mathbf{x}}$-polarized electric field, power is divided evenly among all apertures. (d) Normalized power flowing along the negative z direction as a function of x plotted at $y = z = 0$ (center of the object). Blue and red lines correspond to illumination with $\hat{\mathbf{x}}$-polarized and $-\hat{\mathbf{x}} + \hat{\mathbf{y}}$-polarized waves. In the latter case, only half of the apertures carry energy and therefore the local power is doubled relative to the former case. The gray regions indicate the position of apertures (air). (e) Normalized amplitude and phase of the electric field along the propagation path in the middle of one aperture. Structure is illuminated with an $\hat{\mathbf{x}}$-polarized plane wave. Amplitude of the wave is approximately constant along the propagation path (except for short transition ranges at the beginning and end interfaces of the aperture with free space), and the phase remains virtually linear. Effective wave number of the wave is equal to that of free space, corresponding to the TEM-like nature of the wave inside aperture.

Kerker relation at any interface normal to the direction of wave propagation, i.e., $\epsilon_r(z = z_0) = \mu_r(z = z_0)$ [37,49]. Our proof provides a significantly wider class of structures with similarly zero backscattering. Several near-field evanescent waves may be induced around a self-dual structure, yet from the far-field point of view the effective impedance of the scatterer as a whole is matched with free-space.

While the previous example and the related discussions are general and do not entail a specific distribution of EM waves inside the structure, the composition of the surface can be properly engineered to create many interesting effects. One such case is to achieve extreme funneling, i.e., forcing the EM energy to traverse the slab while being highly localized into linelike channels with deeply subwavelength cross sections. This is shown in Fig. 3(a), where we fill almost the entire cross section of the unit cell with impenetrable perfect conductors, leaving small air apertures for the wave to traverse the structure. As the self-duality condition is satisfied, zero reflection automatically ensures that the entire incident energy must pass through the interface and inevitably though the narrow apertures [Fig. 3(b)]. Interestingly, here the open apertures form waveguides (with deeply subwavelength cross sections) capable of supporting TEM-like propagation modes along the z direction. The local fields inside these waveguides are inversely proportional to the aperture area in each cross section. As shown in Fig. 3(c), each aperture supports its own TEM-like mode with $\pm 45°$ rotated polarizations relative to xy coordinates. Both types of modes are excited (i.e., we see fields in all nine apertures), when the illuminating plane wave is $\hat{\mathbf{x}}$ polarized. However, if the structure is excited with a $\hat{\mathbf{x}} + \hat{\mathbf{y}}$-polarized wave, only half of the apertures would carry power to the other side and the local power would be doubled inside each aperture [Fig. 3(d)]. Conversely, if we illuminate the periodic slab with a $\hat{\mathbf{x}} - \hat{\mathbf{y}}$-polarized wave, the other apertures would carry the energy.

Interestingly, only small regions of near-field coupling at the incident interface (i.e., at $z = t/2$) and the outgoing interface (i.e., at $z = -t/2$) are observed [Figs. 3(b) and 3(e)]. When all the apertures are similar, the outgoing wave follows the same polarization as the input one. As discussed in the previous example, in principle it should be possible to alter the polarization of the output while maintaining zero reflection. Here, for instance, a simple recipe to that effect would be to change the speed of the wave (i.e., wave number) in half of the apertures supporting the $\mathbf{x} + \mathbf{y}$ polarized wave, compared to the other half that support the $\mathbf{x} - \mathbf{y}$ polarized wave. As a result, one can control the rotation angle and ellipticity of the transmitted wave depending on the thickness of the surface.

Our proposed class of reflectionless slablike structures, along with the presented results on creating arbitrarily shaped EM funnels, independence of the effect from thickness, the nonresonant nature of the phenomenon, and the possibility of managing the polarization of the outgoing wave, demonstrate a powerful concept in controlling EM energy. These characteristics are quite different from the typically ultra-narrow-band transmission attained in EOT-based structures. Rather than relying on precise tuning of leaky surface modes and the evanescent near-field profile, here we achieve matching through an elaborate combination of duality and rotational symmetry, providing us with a newly found freedom in design and a robust performance. We show that self-duality provides a protected form of power transmission that is immune to variations in the geometry and material properties along the propagation path (even for drastic changes along the path as discussed in Ref. [41]). This also brings interesting analogy with the concept of topological protected wave propagation. Adding loss, gain and/or nonlinearity may provide interesting degrees of freedom to design reflectionless absorptive and amplifying surfaces. As shown through the last example, it is possible to create extremely localized power transmission through electromagnetically thick surfaces and potentially across a wide range of frequencies.

This work was supported in part by the Vannevar Bush Faculty Fellowship program sponsored by the Basic Research Office of the Assistant Secretary of Defense for Research and Engineering and funded by the Office of Naval Research through Grant No. N00014-16-1-2029.

*esmo@seas.upenn.edu
†engheta@seas.upenn.edu
‡rkastner@seas.upenn.edu

[1] H. T. Chen, J. Zhou, J. F. O'Hara, F. Chen, A. K. Azad, and A. J. Taylor, Antireflection Coating Using Metamaterials and Identification of Its Mechanism, Phys. Rev. Lett. **105**, 073901 (2010).
[2] P. Spinelli, M. A. Verschuuren, and A. Polman, Broadband omnidirectional antireflection coating based on subwavelength surface Mie resonators, Nat. Commun. **3**, 692 (2012).
[3] M. S. Davis, W. Zhu, T. Xu, J. K. Lee, H. J. Lezec, and A. Agrawal, Aperiodic nanoplasmonic devices for directional colour filtering and sensing, Nat. Commun. **8**, 1347 (2017).
[4] R. Magnusson, Wideband reflectors with zero-contrast gratings, Opt. Lett. **39**, 4337 (2014).
[5] M. Al-Joumayly and N. Behdad, A new technique for design of low-profile, second-order, bandpass frequency selective surfaces, IEEE Trans. Antennas Propag. **57**, 452 (2009).
[6] F. Lu, F. G. Sedgwick, V. Karagodsky, C. Chase, and C. J. Chang-Hasnain, Planar high-numerical-aperture low-loss focusing reflectors and lenses using subwavelength high contrast gratings, Opt. Express **18**, 12606 (2010).
[7] M. Khorasaninejad, W. T. Chen, R. C. Devlin, J. Oh, A. Y. Zhu, and F. Capasso, Metalenses at visible wavelengths: Diffraction-limited focusing and subwavelength resolution imaging, Science **352**, 1190 (2016).

[8] H. Ma, S. Qu, Z. Xu, and J. Wang, Using photon funnels based on metamaterial cloaks to compress electromagnetic wave beams, Appl. Opt. **47**, 4193 (2008).
[9] C. Genet and T. W. Ebbesen, Light in tiny holes, Nature (London) **445**, 39 (2007).
[10] H. A. Bethe, Theory of diffraction by small holes, Phys. Rev. **66**, 163 (1944).
[11] T. W. Ebbesen, H. J. Lezec, H. F. Ghaemi, T. Thio, and P. A. Wolff, Extraordinary optical transmission through sub-wavelength hole arrays, Nature (London) **391**, 667 (1998).
[12] L. Martin-Moreno, F. J. Garcia-Vidal, H. J. Lezec, K. M. Pellerin, T. Thio, J. B. Pendry, and T. W. Ebbesen, Theory of Extraordinary Optical Transmission through Subwavelength Hole Arrays, Phys. Rev. Lett. **86**, 1114 (2001).
[13] F. G. De Abajo, R. Gómez-Medina, and J. J. Sáenz, Full transmission through perfect-conductor subwavelength hole arrays, Phys. Rev. E **72**, 016608 (2005).
[14] M. Beruete, M. Sorolla, I. Campillo, J. S. Dolado, L. Martín-Moreno, J. Bravo-Abad, and F. J. Garcia-Vidal, Enhanced millimeter wave transmission through quasioptical subwavelength perforated plates, IEEE Trans. Antennas Propag. **53**, 1897 (2005).
[15] F. J. Garcia-Vidal, L. Martin-Moreno, T. W. Ebbesen, and L. Kuipers, Light passing through subwavelength apertures, Rev. Mod. Phys. **82**, 729 (2010).
[16] R. Gordon, D. Sinton, K. L. Kavanagh, and A. G. Brolo, A new generation of sensors based on extraordinary optical transmission, Acc. Chem. Res. **41**, 1049 (2008).
[17] S. M. Williams, A. D. Stafford, K. R. Rodriguez, T. M. Rogers, and J. V. Coe, Accessing surface plasmons with Ni microarrays for enhanced IR absorption by monolayers, J. Phys. Chem. B **107**, 11871 (2003).
[18] S. Collin, F. Pardo, and J. L. Pelouard, Resonant-cavity-enhanced subwavelength metal–semiconductor–metal photodetector, Appl. Phys. Lett. **83**, 1521 (2003).
[19] T. Ishi, J. Fujikata, K. Makita, T. Baba, and K. Ohashi, Si nano-photodiode with a surface plasmon antenna, Jpn. J. Appl. Phys. **44**, L364 (2005).
[20] C. Liu, V. Kamaev, and Z. V. Vardeny, Efficiency enhancement of an organic light-emitting diode with a cathode forming two-dimensional periodic hole array, Appl. Phys. Lett. **86**, 143501 (2005).
[21] A. G. Brolo, E. Arctander, R. Gordon, B. Leathem, and K. L. Kavanagh, Nanohole-enhanced Raman scattering, Nano Lett. **4**, 2015 (2004).
[22] A. Lesuffleur, L. K. S. Kumar, A. G. Brolo, K. L. Kavanagh, and R. Gordon, Apex-enhanced Raman spectroscopy using double-hole arrays in a gold film, J. Phys. Chem. C **111**, 2347 (2007).
[23] B. Guo, G. Song, and L. Chen, Plasmonic very-small-aperture lasers, Appl. Phys. Lett. **91**, 021103 (2007).
[24] T. Onishi, T. Tanigawa, T. Ueda, and D. Ueda, Polarization control of vertical-cavity surface-emitting lasers by utilizing surface plasmon resonance, IEEE J. Quantum Electron. **43**, 1123 (2007).
[25] N. Yu, J. Fan, Q. J. Wang, C. Pflügl, L. Diehl, T. Edamura, M. Yamanishi, H. Kan, and F. Capasso, Small-divergence semiconductor lasers by plasmonic collimation, Nat. Photonics **2**, 564 (2008).
[26] H. S. Lee, Y. T. Yoon, S. S. Lee, S. H. Kim, and K. D. Lee, Color filter based on a subwavelength patterned metal grating, Opt. Express **15**, 15457 (2007).
[27] A. Drezet, C. Genet, and T. W. Ebbesen, Miniature Plasmonic Wave Plates, Phys. Rev. Lett. **101**, 043902 (2008).
[28] A. Nahata, R. A. Linke, T. Ishi, and K. Ohashi, Enhanced nonlinear optical conversion from a periodically nanostructured metal film, Opt. Lett. **28**, 423 (2003).
[29] A. G. Brolo, S. C. Kwok, M. G. Moffitt, R. Gordon, J. Riordon, and K. L. Kavanagh, Enhanced fluorescence from arrays of nanoholes in a gold film, J. Am. Chem. Soc. **127**, 14936 (2005).
[30] J. A. H. Van Nieuwstadt, M. Sandtke, R. H. Harmsen, F. B. Segerink, J. C. Prangsma, S. Enoch, and L. Kuipers, Strong Modification of the Nonlinear Optical Response of Metallic Subwavelength Hole Arrays, Phys. Rev. Lett. **97**, 146102 (2006).
[31] M. M. Alkaisi, R. J. Blaikie, S. J. McNab, R. Cheung, and D. R. S. Cumming, Sub-diffraction-limited patterning using evanescent near-field optical lithography, Appl. Phys. Lett. **75**, 3560 (1999).
[32] D. B. Shao and S. C. Chen, Surface-plasmon-assisted nanoscale photolithography by polarized light, Appl. Phys. Lett. **86**, 253107 (2005).
[33] A. Degiron, H. J. Lezec, W. L. Barnes, and T. W. Ebbesen, Effects of hole depth on enhanced light transmission through subwavelength hole arrays, Appl. Phys. Lett. **81**, 4327 (2002).
[34] W. W. Salisbury, U.S. Patent No. 2,599,944, U.S. Patent and Trademark Office, Washington, DC, 1952.
[35] J. P. Berenger, A perfectly matched layer for the absorption of electromagnetic waves, J. Comput. Phys. **114**, 185 (1994).
[36] S. D. Gedney, An anisotropic perfectly matched layer-absorbing medium for the truncation of FDTD lattices, IEEE Trans Antennas Propag. **44**, 1630 (1996).
[37] V. Weston, Theory of absorbers in scattering, IEEE Trans. Antennas Propag. **11**, 578 (1963).
[38] W. Yu, R. Mittra, and D. H. Werner, FDTD modeling of an artificially synthesized absorbing medium, IEEE Microwave Guided Wave Lett. **9**, 496 (1999).
[39] W. Yu, D. H. Werner, and R. Mittra, Reflection characteristic analysis of an artificially synthesized absorbing medium, IEEE Trans. Magn. **37**, 3798 (2001).
[40] O. Vacus and R. W. Ziolkowski, Roughly impedance-matched scatterers constructed with magnetodielectric cells, IEEE Trans. Antennas Propag. **63**, 4418 (2015).
[41] See Supplemental Material at http://link.aps.org/supplemental/10.1103/PhysRevLett.124.033901 for detailed proof of zero backscattering from self-dual bodies as well as discussion on ultrathin self-dual slabs, effect of angular and frequency dispersion on the matching, extreme funneling, and z variant self-dual slabs.

[42] R. F. Harrington, *Time-Harmonic Electromagnetic Fields* (McGraw-Hill, New York,1961).
[43] H. Mott, *Polarization in Antennas and Radar* (Wiley, New York 1986).
[44] N. I. Landy, S. Sajuyigbe, J. J. Mock, D. R. Smith, and W. J. Padilla, Perfect Metamaterial Absorber, Phys. Rev. Lett. **100**, 207402 (2008).
[45] A. Moreau, C. Ciracì, J. J. Mock, R. T. Hill, Q. Wang, B. J. Wiley, A. Chilkoti, and D. R. Smith, Controlled-reflectance surfaces with film-coupled colloidal nanoantennas, Nature (London) **492**, 86 (2012).
[46] S. Yu, X. Piao, and N. Park, Bohmian Photonics for Independent Control of the Phase and Amplitude of Waves, Phys. Rev. Lett. **120**, 193902 (2018).
[47] C. W. Hsu, B. Zhen, A. D. Stone, J. D. Joannopoulos, and M. Soljačić, Bound states in the continuum, Nat. Rev. Mater. **1**, 16048 (2016).
[48] COMSOL Multiphysics 5.3 and 5.4, https://www.comsol.com.
[49] M. Kerker, D. S. Wang, and C. L. Giles, Electromagnetic scattering by magnetic spheres, J. Opt. Soc. Am. **73**, 765 (1983).